Computational Materials Science 150 (2018) 197–201

Contents lists available at ScienceDirect

Computational Materials Science

journal homepage: www.elsevier.com/locate/commatsci

A first principles study of commonly observed planar defects in Ti/TiB system

Peeyush Nandwana[a,1,*], Niraj Gupta[b], Srivilliputhur G. Srinivasan[b,*], Rajarshi Banerjee[b,*]

[a] Materials Science and Technology Division, Oak Ridge National Laboratory, Oak Ridge, TN, USA
[b] Department of Materials Science and Engineering, University of North Texas, Denton, TX, USA

ARTICLE INFO

Keywords:
Titanium
Titanium boride
Interfaces
DFT
NEB

ABSTRACT

TiB exhibits a hexagonal cross-section with growth faults on (1 0 0) planes and contains B27-B_f bicrystals. The hexagonal cross-section is presently explained by surface free energy minimization principle. We show that interfacial energy calculations explain the longer (1 0 0) facet compared to (1 0 1) type facets whereas free surface energy arguments do not provide the true picture. No quantitative explanation of stacking faults and B27-B_f interfaces in TiB exists. We show that the low formation energy of stacking faults and B27-B_f interfaces explain their abundance. The low energy barrier for B_f formation is shown to be responsible for their presence in TiB.

TiB has gained significant attention as an excellent reinforcement in titanium alloys owing to its high strength, comparable density with titanium (4.5 g/cm^3 for Ti compared to 4.46 g/cm^3 for TiB), and high temperature chemical and structural stability in titanium matrix [1–7]. TiB also breaks down the solidification texture, refines as-cast grain size and restricts grain growth of the BCC β phase during hot working of titanium alloys [1,5,8–12]. Furthermore, TiB acts as a heterogeneous nucleation site for the HCP α phase and influences the morphology of α phase cooling from β phase field as widely discussed in literature [5,8–11,13–17].

The microstructural characterization of TiB fabricated via diverse processing routes indicate that it crystallizes in a hexagonal cross section with (1 0 0), (1 0 1), and (1 0 $\bar{1}$) planes as the bounding planes with (1 0 0) plane having the largest area and a high density of stacking faults as shown in Fig. 1(a) [7,18–25]. The hexagonal cross-section has been explained based on arguments that invoke the stoichiometry of Ti and B on the boundary planes or free surface excess energy. Such analyses are incomplete without accounting for interfacial energy because TiB nucleates and grows in an alloy matrix [18,19]. Concurrently, we must also consider stacking fault energy (SFE) given the abundance of these defects. The stacking fault formation has been attributed to the high growth rates of TiB resulting from fast diffusion of small B atoms. Since these faults result from a scarcity of B atoms during the growth of TiB, they are classified as intrinsic faults [19]. Recently, Feng et al. characterized these intrinsic growth faults in TiB in detail and showed that intrinsic faults consist of metastable B_f structure sandwiched between B27 motifs [26]. De Graef et al. also reported the presence of metastable B_f boride phase with Cmcm structure in conjunction with the B27 boride phase with Pnma structure in an earlier study [27]. It was reported that the B_f and B27 structures have a fully coherent interface [20,24,27]. Genç et al. characterized these structures via high resolution microscopy as shown in Fig. 1(b). Despite the prior mentioned observations on growth defects and interfaces in TiB, there is no quantification of the energetics of such abundantly observed defects. Here, we calculate the interfacial energies of TiB/Ti interfaces, and also compare them with previously used surface energy arguments to explain the growth morphology of TiB in Ti matrix. We also present the energetics of B_f-B27 interfaces to explain the faulted TiB structure. Our calculations also provide insights into the ease of formation of B_f structure based on nudged elastic band method (NEB).

First principles calculations were carried out using Vienna Ab-initio Simulation Package (VASP) employing a projected augmented plane wave method [28]. Generalized gradient approximation (GGA) using Perdew-Burke-Erzenhrof (PBE) parameterization was employed for electron correlation function. Mathfessel-Paxton integration scheme with a smearing width of 0.2 eV was used to describe partial occupancies in Brillouin zone. The plane wave cut off energy of 500 eV was used in all calculations. A Monkhorst-Pack k-mesh of 3 × 5 × 3 was used for B27 and B_f symmetries of TiB single crystals. The atom positions were relaxed to a force of less than 0.02 eV/Ang. The same parameters were used to determine relaxed energy value for α Ti single crystal. The calculated lattice parameters for TiB B27, TiB B_f, and α – Ti

* Corresponding authors.
E-mail address: nandwanap@ornl.gov (P. Nandwana).
[1] Note: Author P. Nandwana was at University of North Texas during a major part of this work.

https://doi.org/10.1016/j.commatsci.2018.04.006
Received 18 August 2017; Received in revised form 4 April 2018; Accepted 5 April 2018

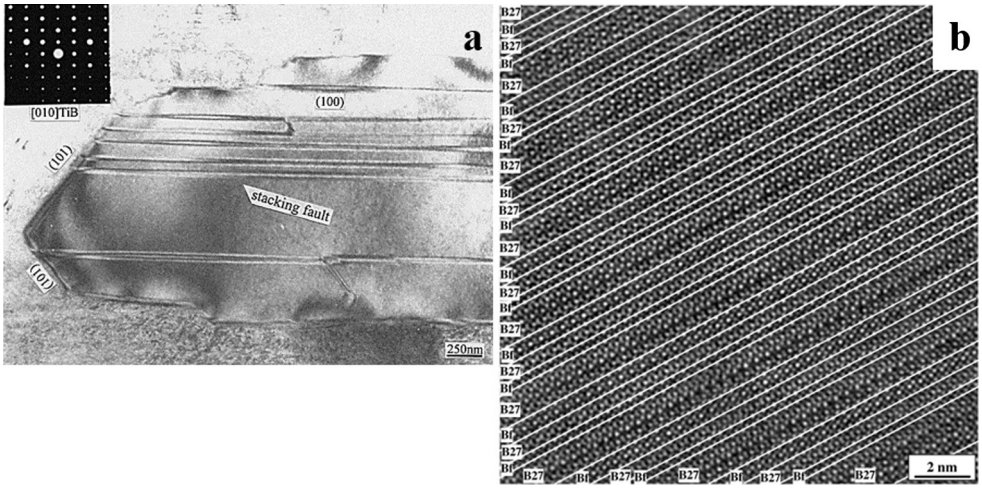

Fig. 1. (a) Hexagonal cross-section of TiB with stacking faults on (1 0 0) plane imaged along [0 1 0] zone axis, and (b) co-existence of the B27-B_f structures in TiB [19,20].

Table 1
Experimental lattice parameters of B27 TiB, B_f TiB, and α-Ti are compared with their corresponding DFT values.

Phase	Symmetry	DFT (Å)	Experimental (Å) [27,31]
TiB	B27	a = 6.118, b = 3.055, c = 4.567	a = 6.12, b = 3.06, c = 4.55
TiB	Bf	a = 3.286, b = 8.487, c = 3.055	a = 3.23, b = 8.56, c = 3.05
α-Ti	$P6_3/mmc$	a = 2.937, c = 4.659	a = 2.95, c = 4.68

agree well with the experimentally determined parameters as seen in Table 1. A k-mesh of 1 × 5 × 3 was used for the free surface energy and interfacial energy calculations. The interface structures employed for the current study are discussed in detail in subsequent sections. For the interfacial energy calculations, the threshold for energy convergence was 1×10^{-5} eV and the atoms were relaxed to forces smaller than 0.005 eV/Ang. For NEB calculations conducted to determine the energy barriers for B27-B_f formation, the structures were fully relaxed to 0.02 eV/Ang force per atom.

TiB precipitate in α Ti matrix has a hexagonal cross-section whose facets are indexed as (1 0 0), (1 0 1), and (1 0 $\bar{1}$) planes. Typically, the (1 0 0) facet is considerably longer than the (1 0 1) type facets as shown in Fig. 1(a). Attempts have been made to explain this observation on the basis of surface free energy minimization criterion [29]. However, no quantitative data is available for the free surface energies of various TiB planes. Thus, we first calculated the surface energies of bounding planes of TiB by employing slab models of surfaces created using MedeA™. Most of the surfaces were terminated by Ti atoms to maintain the stoichiometry of the crystal, the only exception being the (1 0 0) TiB surface that can either be terminated in Ti or B atoms, still allowing for the stoichiometry to be maintained. Fig. 2(a) and (b) respectively show the Ti terminated (1 0 0) surface and a stoichiometric (0 0 1) surface. A vacuum gap of 10 Å was kept on either side of the surfaces to minimize their interaction with each other across the box boundaries. The system was allowed to undergo full relaxation including ionic rearrangements to promote surface reconstructions. The surface energy (γ) was calculated using

$$\gamma = \{E - (N * \mu_{TiB})\}/(2 * A) \quad (1)$$

Here, E is the energy of the surface system, N is the number of TiB pairs, μ_{TiB} is the reference energy of one TiB pair in the bulk crystal, and A is the surface area. The reference energy of TiB (−16.2385 eV) was calculated by relaxing a TiB unit cell to minimum energy configuration at 0 K. Table 2 presents the surface energy values for free surfaces in

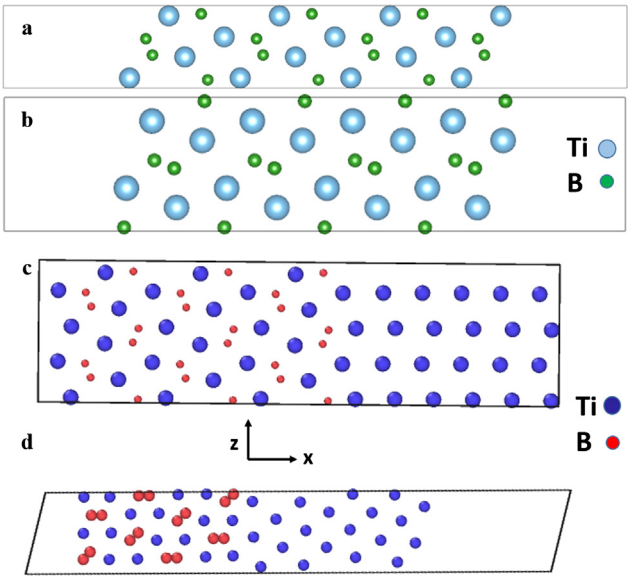

Fig. 2. (a) Ti terminated (1 0 0) surface and (b) stoichiometric (0 0 1) surface, both with vacuum gaps of 10 Å, (c) $(1\,0\,0)_{TiB}||(10\text{-}10)_a$ and (d) $(1\,0\,1)_{TiB}||(10\text{-}10)_a$ interfaces projected along $[0\,1\,0]_{TiB}||[11\text{-}20]_a$ axis.

Table 2
Free surface energy of different planes in TiB and its dependence on the terminating atom are presented.

Plane	Surface Energy (mJ/m^2)	Terminating Atom for the Surface
(1 0 0)	4430	B
(1 0 0)	3520	Ti
(0 1 0)	3140	Ti
(0 0 1)	2930	Ti and B
(1 0 1)	2830	Ti
(10-1)	2830	Ti

vacuum for the commonly observed planes of TiB. The calculated energy values show that the (1 0 1) type surfaces have the lowest surface energy followed by (0 0 1), (0 1 0), and (1 0 0) surfaces. Based on the surface energy calculations, the bounding planes should be (1 0 1), (1 0 $\bar{1}$), and (0 0 1) planes. However, this observation is in contrast with the experimentally observed bounding planes i.e. (1 0 0), (1 0 1), and (1 0 $\bar{1}$) [18]. Although, surface energy arguments can partially explain the formation of bounding places, they do not provide the full picture